Article

Poly(vinyl alcohol)/Gelatin Scaffolds Allow Regeneration of Nasal Tissues

Delfo D'Alessandro [1], Stefania Moscato [2], Alessandra Fusco [3], Jose Gustavo De la Ossa [1], Mario D'Acunto [4], Luisa Trombi [2], Marta Feula [5], Lorenzo Pio Serino [1], Giovanna Donnarumma [3], Mario Petrini [2], Stefano Berrettini [1] and Serena Danti [5,*]

[1] Department of Surgical, Medical, Molecular Pathology and Emergency Medicine, University of Pisa, 56126 Pisa, Italy; delfo.dalessandro@unipi.it (D.D.); josegustavo.delao@student.unisi.it (J.G.D.l.O.); lorenzopio.serino@gmail.com (L.P.S.); s.berrettini@med.unipi.it (S.B.)

[2] Department of Clinical and Experimental Medicine, University of Pisa, 56126 Pisa, Italy; stefania.moscato@unipi.it (S.M.); l.trombi@yahoo.it (L.T.); mario.petrini@med.unipi.it (M.P.)

[3] Department of Experimental Medicine, University of Campania "Luigi Vanvitelli," 80138 Naples, Italy; alessandra.fusco@unicampania.it (A.F.); giovanna.donnarumma@unicampania.it (G.D.)

[4] Consiglio Nazionale delle Ricerche, Istituto di Biofisica, CNR-IBF, 56124 Pisa, Italy; mario.dacunto@ibf.cnr.it

[5] Department of Civil and Industrial Engineering, University of Pisa, 56122 Pisa, Italy; martafeula@gmail.com

* Correspondence: serena.danti@unipi.it; Tel.: +39-050-2217874

Featured Application: In this work, we provide a platform for nasal tissue regeneration, consisting of poly(vinyl alcohol)/gelatin sponges and mesodermal progenitor cells as a single stem cell source for connective and vascular tissues. These scaffolds show promise for application in rhinoplasty, as well as nasal tissue reconstruction following sinonasal tumor resection.

Abstract: Need for regeneration and repair of nasal tissues occurs as a consequence of several pathologies affecting the nose, including, but not limited to infective diseases, traumas and tumor resections. A platform for nasal tissue regeneration was set up using poly(vinyl alcohol)/gelatin sponges with 20%–30% (w/w) gelatin content to be used as scaffolds, for their intrinsic hydrophilic, cell adhesive and shape recovery properties. We propose mesodermal progenitor cells (MPCs) isolated from the bone marrow as a unique stem cell source for obtaining different connective tissues of the nose, including vascular tissue. Finally, epithelial cell immune response to these scaffolds was assessed in vitro in an environment containing inflammatory molecules. The results showed that mesenchymal stromal cells (MSCs) deriving from MPCs could be used to differentiate into cartilage and fibrous tissue; whereas, in combination with endothelial cells still deriving from MPCs, into pre-vascularized bone. Finally, the scaffold did not significantly alter the epithelial cell response to inflammatory insults derived from interaction with bacterial molecules.

1. Introduction

As a sensory organ, the nose is physiologically complex and anatomically variegated by its nature. Through our breathing organs, the nose primes the flow of air, which is humidified, heated and filtered right inside. Remarkably, the olfactory function is ascribed to this organ [1]. From an anatomical point of view, different tissue types are present in the nose including cartilage, bone, fibrous, muscle, adipose, and epithelial, which are structurally interconnected with each other through ligaments of different thickness. The integrity of all the anatomical components is essential for the respiratory function [2–4].

The cartilaginous component, of the hyaline type, gives rise to the septum that divides the nose into two cavities; it also constitutes both upper and lower lateral cartilages [5].

The nasal septum acts as a support for the other nose structures to confer rigidity, thus preventing its permanent deformation. Through the lateral cartilages, the nose interfaces with the nasal bones, such as the vomer, the perpendicular plate of ethmoid bone, and incisive bone, which determine nose anchoring to the facial structures [4,6]. Proceeding from the surface to the depth of the nose, a series of layers are present, made up of different tissues devoted to stability and protection against mechanical shocks along with ensuring the correct organ function: the adipose panniculus, the fibromuscular layer rich in vessels, muscles and ligaments, the deep adipose layer and the muco-perichondrium [7–9]. Furthermore, two fibrocartilaginous sacs have recently been identified, one right and one left, linked to the development of nasal cartilages and containing, in their walls, the olfactory mucosa [3].

Given its filtering function and its position, the nose is exposed to a series of injuries of traumatic, chemical, inflammatory and tumorigenic origin [4]. The most common injuries are septal deformations, which cause obstructions of the airways. In addition, nose is subject to tumors, rare but extremely variegated in nature, whose resection causes profound alterations in the cartilaginous structures. Surgery is necessary to repair the damaged anatomical tissues, which, depending on the injury, may require subsequent revisions [10,11]. The surgical procedures currently employed are rhinoplasty and septoplasty, which often exploit cartilaginous grafts to repair damaged structures [2]. The gold standard is autologous cartilage obtained from the septum itself, the auricle or the ribs. The first site is easily accessible, but the amount that can be recovered is limited; on the contrary, plenty of material can be taken from the ribs, but the removal procedure causes donor site morbidity [12–14]. As an alternative, it is possible to use allogeneic grafts. Even though their actual immunogenicity is not known, the limited cellular phase present in cartilage suggests a limited risk [15,16]. Finally, it is possible to apply synthetic materials, which can be molded into the desired shapes, they are cheap and implantable in a single procedure; however, they can lead to sustained inflammation up to device extrusion [17,18]. Thus, an effective and simple reconstructive procedure with minimal side effects has yet to be developed.

A novel approach to nasal reconstruction is shown by tissue engineering (TE). Some studies have proposed biocompatible scaffolds based on decellularized cartilage, collagen, polycaprolactone (PCL), poly(L-lactic) acid (PLLA), poly (lactic-co-glycolic) acid (PLGA) [19–22], and stem cells, such as mesenchymal stromal cells (MSCs), easy to isolate and already used in clinical procedures, or septal chondrocytes [23–25]. Injectable fibrin scaffolds containing septal chondrocytes have been applied directly into the damaged site [26], and constructs fabricated by 3D printing, with the desired shapes, have also been developed [27]. Although these studies gave rise to interesting results in vitro, in animals and recently also in humans, currently no TE construct has been proposed that is able to regenerate all the anatomical structures of the nose [28]. With the aim of further investigating in this field, several materials different from those tested so far could be tested. In this regard, polyvinyl alcohol (PVA) represents a valuable candidate due to its compatibility with many cells and tissues, non-toxicity and non-tumorigenicity, along with its hydrogel-forming capability, which leads to high water contents, similar to that of natural cartilage [29].

In our recent studies, we showed that PVA-based sponges retain some key features of PVA hydrogels, being also able to widely modulate pore size to accomplish different cells and tissue structures [30], thus becoming an interesting scaffold also in the otolaryngological field. By virtue of its hydrophilic nature, PVA can be easily blended with several biomolecules [31]. PVA/gelatin (G) sponges, with highly interconnected pores, allow a good diffusion of nutrients and a high cell penetration. MSCs have demonstrated to differentiate into chondrocytes producing typical molecules of the cartilage extracellular matrix (ECM), both using traditional or scaffold-mediated culture methods [32,33]. These constructs subjected to mechanical stimulation in a bioreactor were also able to generate cartilage with elastic fibers, important for the reconstruction of the auricle [34].

Finally, PVA/G sponges seeded with both bone marrow MSCs, differentiated into osteogenic lineage, and human umbilical vein endothelial cells (hUVECs), terminally differentiated towards endothelial lineage, showed first evidence of vascularized bone generation. This is important, in perspective, to improve implant viability during the regenerative process in vivo [35]. MSCs can differentiate into all mesodermal tissues; however, an efficient differentiation into the endothelial phenotype is still a subject of investigation [36]. The mesodermal (or mesangiogenic) progenitor cells (MPCs) are bone marrow precursors of the MSCs, which, being a step upstream in the mesengenic process, still have a strong potency for vasculogenesis [37,38]. Having a single cellular source to generate the most important structural tissues of the nose, including, but not limited to cartilage, bone, and vasculature, could definitively offer improved therapeutic solutions. Fibrocartilage is a tissue rich in type I collagen fibers, containing few chondrocytes; the fibers are organized in very dense bundles that make the fabric highly resistant to compression. It is a transition tissue between hyaline cartilage and dense connective tissue, typical of ligaments, also determinant for holding the nasal structures together and anchoring them to the face bones [39].

The aim of this study was to create a simple platform of three-dimensional (3D) cell/scaffold constructs for the regeneration of different nasal tissues by a single scaffold, the PVA/G sponge, and a single source of patient's cells, the MPCs, able to generate different cell progenies: chondrogenic, osteogenic, endothelial and fibroblastic. We thus focused on the achievement of 3D constructs allowing the regeneration of hyaline cartilage, vascularized bone and fibrocartilage, which are the main connective tissues in the nose. Obtaining these constructs could represent a relevant step forward in repairing the variegated set of injuries affecting the different anatomical structures of the nose.

2. Materials and Methods

2.1. Materials

Polyvinyl alcohol (PVA; 99% hydrolyzed, Mw 85,000–146,000), Sodium Lauryl Sulphate (SLS), Phosphate buffered saline (PBS), Dulbecco's Modified Eagle Medium (DMEM), Dulbecco's Modified Eagle Medium Low Glucose (DMEM-LG), DMEM/F12, Insulin-transferrin-selenium (ITS), Pyruvate sodium, Dexamethasone, Trypsin, Nuclear fast red, Silver nitrate, Pyrogallole, Sodium Thiosulphate, Gelatin (G; type B from bovine skin), Glycine, Glutaraldehyde (GTA) grade II, L-Glutamine, Penicillin, Streptomycin, Xylene, Triton X-100, Bovine serum albumin (BSA), Mayer's hematoxylin solution, Eosin, Dibutylphthalate Polystyrene Xylene (DPX) mounting medium, Methanol, Proteinase K, Pepstatin A, Iodoacetamide, Dimethylmethylene blue (DMMB), Ethylene Diamino Tetracetyc Acid (EDTA), Ampicillin, Fungizone, Gentamicin, b-glycerophosphate and $MgCl_2$ were purchased from Sigma-Aldrich (Milan, Italy); Diflucan was purchased from Pfizer (Rome, Italy); Minimum Essential Medium, alpha modification was purchased from Cambrex/BioWhittaker (Walkersville, MD, USA); Human fibronectin and Matrigel® were purchased from BD Bioscience (Erembodegem, Belgium); Absolute ethanol and aluminum sulfate were bought from Carlo Erba (Milan, Italy); Citrate buffer was purchased from Diapath (Bologna, Italy); Ficoll Paque Plus, was purchased from GE healthcare (Hatfield, UK); StemMACS ChondroDiff Medium and Endocult were supplied by StemCell Technologies (Vancouver, Canada); Chromogen substrate 3-3′ diaminobenzidine tetrahydrochloride (DAB) was purchased from Amresco (Solon, OH, USA); Neutral buffered formalin and Alcian Blue kit, were purchased from Bio-Optica (Milan, Italy); Paraffin Histoplast LP and TrypLE Select were obtained from Thermo Fisher Scientific (Waltham, MA, USA); Transforming growth factor beta 1 (TGF-β1) was purchased from PeproTech (Rocky Hill, New Jersey); Vascular endothelial growth factor (VEGF) was purchased from Miltenyi Biotec (Cologne, Germany); AB human sera, Roswell Park Memorial Institute (RPMI-1640) medium and Osteogenic differentiation medium were purchased from Lonza (Basel, Switzerland); Heat-inactivated fetal bovine serum (FBS), Fetal Calf Serum (FCS) and Ascorbic acid were bought from Invitrogen (Carlsbad, CA, USA); PicoGreen kit was purchased from

Molecular Probes (Eugene, OR, USA); Normal Goat Serum, Goat anti-mouse secondary antibody, Goat anti-rabbit secondary antibody and Vectastain Elite ABC Kit Standard were purchased from Vector Lab (Burlingame, CA, USA); mouse monoclonal anti-collagen type II (sc52658), rabbit polyclonal anti-Sox-9 (sc-20095), mouse monoclonal anti-Aggrecan (sc-33695), mouse monoclonal anti-Flk-1 (sc-6251), rabbit polyclonal anti-p-Flk-1 (sc-101820), mouse monoclonal anti-PECAM-1 (sc-81158), mouse monoclonal anti-Alkaline Phosphatase (ALP, sc-166261) and rabbit polyclonal anti-Osteocalcin (sc-30044) were obtained from Santa Cruz Biotechnologies (Santa Cruz, CA, USA); rabbit polyclonal anti-collagen type I (ab34710) was purchased from AbCam (Cambridge, UK). LC Fast Start DNA Master SYBR Green kit and Tri Reagent®, LPS e LTA were purchased from Sigma-Aldrich (Merck KGaA, Darmstadt, Germany).

2.2. Ethical Statement

Immortalized human keratinocytes, HaCaT cell line, were commercially obtained from ATCC-LGC Standards (Milan, Italy). Rat MSCs (rMSCs) were collected from discarded tissue from healthy rats sacrificed as controls in other studies approved by the local Ethical Committee. The experimental protocol followed the Principles of Laboratory Animal Care and specifically the re-use principle of the 3Rs. Human MPCs and human MSCs (hMSCs) were obtained by collecting the bone marrow overflowing from the medullary canal (i.e., discarded material) during prosthesis insertion in total hip replacement surgery of orthopedic patients. The samples were treated anonymously and in conformity to the principles expressed by the Declaration of Helsinki. As we used discarded anonymous material otherwise destinated to be disposed, ethical approval was not required.

2.3. Fabrication of PVA/G Sponges

Bioartificial PVA/G sponges were fabricated via emulsion and freeze-drying followed by chemical crosslinking. Specifically, an 11.72% aqueous solution of PVA prepared via autoclaving 1 h at 121 °C was cooled down to 50 °C under stirring at 1000 rpm in a glass flask placed inside a thermostatic bath. G was added to the PVA solution to reach a 20:80 w/w and 30/70 w/w ratio between the biomolecule G and the synthetic polymer PVA. A soft paste was obtained heating up the mixture to 71 °C for 10 min. Thereafter, the bath was cooled down again to 50 °C, 0.36% (w/v) of SLS was added to the mixture and stirring at 1000 rpm was continued for 10 min, leading to the obtainment of a voluminous dense foam that was spread on petri dishes with a large spatula, frozen at −80 °C and lyophilized. The dried foams were stabilized by crosslinking via GTA vapors for 72 h at 37 °C in a sealed cabinet and then flushed under the chemical hood for 48 h, thus obtaining biostable sponge-like materials. The crosslinking efficacy was tested by verifying the structural stability of the matrices in water for 7 days at 37 °C. The PVA/G sponge fabrication method is reported in detail in a previous study [40].

2.4. Morphology and Surface Analysis of PVA/G Sponge

Scanning electron microscopy (SEM) was used to analyze the architectural features of the plain scaffolds. Samples were observed as obtained, post-dried (using either lyophilization or vacuum heating and after mechanical compression). The specimens were cross-sectioned, mounted on aluminum stubs, sputter-coated with gold (Edwards Sputter Coater S150B, Edwards, NY, USA) and examined under a scanning electron microscope JEOL JSM-5600 LV (Jeol Ltd., Tokyo, Japan) with an accelerating voltage of 12 kV.

The surface roughness analysis of lyophilized sponges was carried out with an atomic force microscope (AFM) (Molecular Imaging, TX, USA) equipped with silicon tips (nominal radii 10–20 nm) in air at 20 °C and 40% relative humidity. The analysis was performed working on tapping or contact mode and consisted of topographic data recording of square areas of approximately 40×40 μm^2 (1024×1024 pixels). The roughness data were processed as the average among 15 different areas randomly selected upon the investigated surface.

2.5. Porosity and Pore Features of PVA/G Sponge Surfaces

Micro Computer Tomography (MicroCT) is a non-disruptive method recently used to measure 3D porosity and pore interconnectivity of scaffolds. A parallelepiped scaffold was scanned with a microCT imaging system (SkyScan 1172; SkyScan, Aartselaar, Belgium). Data were acquired and analyzed as previously reported [37,38]. Briefly, the raw micrographs were reconstructed using a Feldkamp algorithm. Then, grayscale thresholds of 45 (lower) and 255 (upper) were selected to have a realistic correspondence between grayscale tomograms and their binarized representations. Representative 3D reconstructions of the samples were generated to show a 3D model of the scaffold. Quantitative data were calculated considering a cylindrical volume of interest (VOI) within the boundaries of the scaffold. The total VOI selected in this study was 1.373 cm^3. Scaffold porosity was obtained using Equation (1):

$$\% \text{ Porosity} = \left(1 - \frac{V_{\text{bin obj}}}{\text{VOI}}\right) \cdot 100\% \tag{1}$$

in which $V_{\text{bin obj}}$ is the binarized object volume within the total VOI. Thereafter, the scaffold interconnectivity was calculated as the void volumetric fraction accessible from the outside through pore openings of a predefined size [37,38]. In this study, a cut-off size of 4 voxels, equal to 51.2 µm, was defined as dimensionally compatible with MSC migration. The interconnected volume was estimated via a "shrink-wrap" process, as reported in the CT Analyzer instructions. The percentage of inaccessible volume can be finally determined in Equation (2), as:

$$\% \text{ Inaccessible Volume} = \left(\frac{\text{VOI}_{\text{POST}} - V_{\text{bin obj,POST}}}{\text{VOI}_{\text{PRE}} - V_{\text{bin.obj,PRE}}}\right) \cdot 100 \tag{2}$$

Here, the terms POST and PRE refer to after and before the shrink-wrap process, respectively. Finally, interconnectivity percent can be calculated as the complement to the inaccessible volume percent.

2.6. Water Content and Mechanical Characterization of PVA/G Sponges

A lyophilized sponge was puncher-cut into cylinders ($n = 6$) with diameter (D) = 8 mm and height (H) ranging in 4.2–4.8 mm, as measured with an electronic caliper (Mitutoyo, Tokyo, Japan). The specimens were equilibrated in PBS (PBS; Sigma-Aldrich) 0.1 M, pH 7.4, for 2 h at 37 °C. Excess of liquid was carefully removed leading to the evaluation of their wet weight (V_{wet}). The wet sponges were placed under a laminar flow hood for 3 days. The volume increase percent were calculated with respect to the wet and dry conditions, using Equation (3), in which *wet* refers to either wet or post-dry volume condition.

$$\% \text{ Volume Increase} = \frac{\left(V_{\text{wet}} - V_{\text{dry}}\right)}{V_{\text{dry}}} \cdot 100\% \tag{3}$$

A bench dynamometer (INSTRON 5542, 50 N load cell, UK) was used to test samples in unconfined compression between two 50 mm diameter non-porous stainless-steel platens. Six samples, previously subjected to the above-described water content analysis, underwent a compressive ramp up to 50% strain at a strain rate of 0.0167 mm/s. Some drops of double-distilled water were placed around the samples to ensure that they remained hydrated throughout testing. The tangent slope was measured by calculating a baseline estimate for localized data at 10% increments from 10% to 50% strain.

2.7. Isolation and Expansion of Bone Marrow Stem Cells

This study availed itself of bone marrow-derived stem cells of rat and human origin. Mononuclear cells were collected from human bone marrow aspirates by density gradient centrifugation on Ficoll-Paque Plus, and plated in DMEM-LG supplemented with 10% of pooled human AB sera at $0.8 \times 10^6/cm^2$ on hydrophobic untreated flasks. After 48–72 h,

nonadherent cells were discarded and fresh medium was added. After 8–10 days, the cells were detached with TrypLE Select for 15–20 min at 37 °C, in 5% CO_2 cell incubator obtaining MPCs, a bone marrow stem cell population resting and more immature than MSCs, able to differentiate towards the mesenchymal and endothelial lineages. HMSCs were thus obtained from human MPCs by replacing human AB serum with FBS, as reported in previous studies [41]. HMSCs cultured using DMEM-LG supplemented with 10% FBS, 100 IU/mL penicillin, 100 μg/mL streptomycin, 2 mM L-glutamine, 100× Diflucan (2 mg/mL). Cells were seeded at a density of 200,000 cells/cm^2 and cultured in in 5% CO_2 cell incubator. After 48–72 h nonadherent cells were discarded and fresh medium was added. When 80% confluence was reached adherent cells were trypsinized and seeded at low density for further expansion.

Finally, rMSCs were harvested from the tibiae and femora of 41–44-days-old male Wistar rats (Charles River Laboratories, USA) using established method as previously described [42]. Briefly, the leg bones were excided, the soft tissue was removed, and the leg bones were placed in DMEM supplemented with 200 μg/mL of PSF cocktail. This concentration of antibiotics is 4 times superior to the normal concentration used in cell culture to avoid contamination during the harvest process. The proximal end of the femur and distal end of the tibia were clipped. An 18-gauge needle was inserted into the hole in knee joint in each bone, and the bone was flushed with 5 mL of complete osteogenic medium (α-MEM supplemented with 10% FBS, 50 μg/mL gentamicin, 100 μg/mL ampicillin, 10 mM fungizone, 50 μg/mL L-ascorbic acid, 0.01 M β-glycerophosphate, and 0.01 M dexamethasone). The resulting marrow pellet was broken up by trituration, and cell suspensions from all bones were combined in a centrifuge tube. The cells were plated in 75 cm^2 flasks and cultured for 6 days in complete osteogenic media at 37 °C in a humidified atmosphere of 95% air, 5% CO_2 to allow the expansion of the cells. Medium was changed at 1 and 3 days to remove the non-adherent cell population.

2.8. PVA/G Scaffold Preparation and Generation of 3D Models

The sponges, 80/20 and 70/30 (*w*/w%) PVA/G, were puncher cut into cylinders (5 mm diameter, 3 mm or 1.5 mm thickness) that were sterilized with absolute ethanol overnight, washed three times, 10 min each, with sterile 3× Pen-Strep/Diflucan in saline, rinsed in sterile PBS and finally treated with a sterile-filtered 2 M aqueous solution of glycine for 1 h to block GTA unreacted binding sites. Thereafter, the scaffolds were washed with sterile PBS to remove excess glycine prior to cell seeding.

2.8.1. Chondrogenic Differentiation of MSCs in PVA/G Scaffolds

RMSCs at passage 2 were seeded on 80/20 (*w*/w%) PVA/G scaffolds (3 mm thickness) at a density of 500,000 cells/sample using regular culture medium for adhesion. After 24 h, the cell/scaffold constructs were committed to the chondrogenic lineage, replacing the regular culture medium with differentiating culture medium, consisting of DMEM:F12, 1.25 μg/mL bovine serum albumin, 5.35 μg/mL linoleic acid, 50 μg/mL ascorbic acid, 100 μg/mL sodium pyruvate, ITS, 10^{-7} M dexamethasone and 10 ng/mL and TGF-β1. Differentiation was carried out for 10 days and 20 days, providing culture medium changes every 3 days.

2.8.2. Vasculogenic and Osteogenic Differentiation of MPCs in PVA/G Sponges

To perform pre-endothelial differentiation, MPCs were plated at 10,000 cells/cm^2 in Endocult differentiation medium on 25 cm^2 tissue culture flasks coated with human fibronectin and cultured for 2–3 weeks. Pre-endothelial cells were then detached with trypsin digestion and counted to seeding them on scaffolds. Parallel cultures were performed on chamber slides previously coated with Matrigel® (100 μL/well) to obtain terminal differentiation. After 18 h, chamber slides were fixed in 1% *w/v* neutral buffered formalin for 10 min at 4 °C. In the meantime, the 80/20 (*w*/w%) PVA/G scaffolds (1.5 mm thickness) were seeded with hMSCs at the density of 500,000 cell/scaffold and the con-

structs were osteodifferentiated for 14 days using OsteoDiff Medium. Osteoblast/PVA constructs were then coated with Matrigel (100 μL/scaffold) and MPC-derived pre-endothelial cells obtained from Endocult cultures were seeded at the density of 400,000 cell/scaffold. Terminal endothelial differentiation was performed by incubating the constructs in Endocult medium containing 50 ng/mL of VEGF in cell culture incubator for 18 h.

2.8.3. Fibrocartilaginous Differentiation of MSCs in PVA/G Scaffolds

HMSCs at passage 2 were trypsinized and seeded in 75 cm^2 flasks at a density of 5000 cells/cm. After 4 days of expansion in DMEM, cells were committed to chondrogenic lineage by adding StemMACS ChondroDiff Medium and pre-differentiated for 4 days. After the pre-differentiation in 2D conditions, the chondroprogenitor cells were trypsinized, seeded on 70/30 (*w*/*w*%) PVA/G scaffolds (1.5 mm thickness) at a density of 300,000 cells/sample and differentiated for additional 24 days.

2.9. 3D Model Characterization
2.9.1. Histological Characterization of 3D Models

After formalin fixation, constructs employed to the creation of chondrogenic, vascularized osteogenic and fibrocartilaginous models were dehydrated with a graded series of ethanol (from 70% to 100%). After 3 h of incubation in absolute ethanol (Bio-Optica), samples were clarified in xylene (two steps of 45 min each) (Sigma-Aldrich). All steps were performed in a thermostatic bath at 40 °C. Successively, specimens were rinsed in liquid paraffin (Histoplast LP, Thermo Fisher Scientific, Waltham, MA, USA) at 60 °C for 2 h and paraffin-embedded. Sections 5 μm thick were obtained by standard microtome and mounted onto glass slides. Before each histological staining or immunoreaction, sections were deparaffined in xylene (two steps of 7 min each), rehydrated in absolute ethanol (three steps of 7 min each) and rinsed in distilled water for 5 min. Before each staining, sections of both seeded PVA and chondrogenic pellet were deparaffinized; after each staining, the sections were dehydrated.

- Hematoxylin and Eosin (H&E) staining

Sections were deparaffinized rinsing them in xylene twice for 7 min, then they were rehydrated by absolute ethanol three times for 7 min and washing them in distilled water for 5 min. Samples were then stained with Mayer's hematoxylin for 5 min, washed in tap water for 5 min and counterstained with 1% *w/v* eosin for 1 min. After washing in distilled water, specimens were dehydrated by three washes in absolute ethanol and clarified by three washes in xylene (5 min for each step), then they were mounted with a coverslip by DPX mounting agent.

- Alcian Blue pH 1 staining

Specimens were incubated in Alcian Blue pH 1 solutions for 30 min and in revealing solutions for 10 min, according to manufacturer's instructions. After the incubation time, sections were washed in distilled water, counterstained with a distilled water solution containing 0.1% *w/v* Nuclear Fast Red and 5% *w/v* aluminum sulfate for 5 min and washed in tap water for 5 min. Sections were dehydrated and mounted as previously described.

- Von Kossa staining

Deparaffinized sections were incubated with 1% *w/v* silver nitrate exposed to light for 15 min, 0.5% *w/v* Pyrogallol for 2 min and 5% *w/v* sodium thiosulphate for 2 min. All the solutions were made in distilled water. After each passage, washings in distilled water were performed. The counterstaining was performed by incubating cells with 0.1% *w/v* nuclear fast red diluted in a distilled water solution containing 5% *w/v* aluminum sulphate, for 5 min and washing in tap water for 5 min in order to reveal the reaction. Sections were dehydrated and mounted as previously described.

- Immunohistochemical analysis

Sections employed for the detection of aggrecan and collagen type II were incubated in citrate buffer in a thermostatic bath at 90 °C for 30 min, in order to unmask antigens, then they were cooled down for 30 min and washed in $1\times$ PBS for 10 min; cells and sections employed for the detection of the other antigens were permeabilized with 0.2% *w/v* Triton X-100 in $1\times$ PBS for 10 min. All specimens were incubated in a methanolic solution containing 0.06% *v/v* H_2O_2 in the dark for 15 min to quench peroxidases. Sections were rinsed in distilled water and washed in $1\times$ PBS. Therefore, specimens were incubated with 5% *v/v* goat serum diluted in 1x PBS for 20 min at 37 °C to block aspecific binding sites of the secondary antibodies. Specimens were washed in 1x PBS and then incubated with primary antibodies diluted in 0.1% *w/v* BSA/1x PBS solution in a moist chamber overnight at 4 °C. The following antibodies with specified concentrations were used: anti-aggrecan 1:50; anti-Sox-9 1:100; anti-collagen type II 1:50, anti-collagen type I 1:1000, anti-ALP 1:100, anti-Osteocalcin 1:400, anti-TGFβ-1 1:100, anti-Flk-1 1:50, anti-p-Flk-1 1:50, anti-PECAM-1 1:100. Negative controls were obtained by incubating some sections with 0.1% *w/v* BSA/1x PBS only. The next day, specimens were incubated with goat anti-rabbit or goat anti-mouse biotinylated secondary antibodies diluted 1:200 in 1.5% *v/v* goat serum-1x PBS solution for 60 min, then streptavidin solution was added for 30 min, prepared according to manufacturer's instructions reported in the Vectastain Elite ABC Kit Standard. To reveal the reaction, the sections were incubated in the substrate-chromogen solution (0.5 mg/mL 3,3′-diaminobenzidine tetrahydrochloride activated by H_2O_2) for 5 min in the dark, then they were counterstained with Mayer's hematoxylin for 2 min and washed in tap water for 2 min. Finally, the sections were dehydrated, clarified and mounted in DPX medium. In the second part of the reaction, after each passage, washings in 0.01% *v/v* Triton/PBS $1\times$ and $1\times$ PBS solutions were performed. All the histological analyses were observed with a Nikon Eclipse Ci microscope (Nikon Instruments, Amsterdam, the Netherlands) and the images were acquired by a digital camera equipped on the microscope.

2.9.2. Morphological Analysis of Chondrogenic 3D Model

- SEM analysis

After fixation and washing in $1\times$PBS, constructs employed to the creation of the chondrogenic model were dehydrated with a graded series of ethanol ethanol/water solutions up to anhydrous ethanol. The specimens were dried using the critical point method (Balzers CPD030, Oerlikon Balzers, Balzers, Liechtenstein), then mounted on aluminum stumps, sputter-coated with gold and examined using a scanning electron microscope as previously reported.

- Rounded cell evaluation

To evaluate the tendence of rMSCs to form groups in the chondrogenic model, rounded total cells (RTC) and rounded cell groups (RCG) were counted in nine histological sections; sections were collected one each 10–15 μm from sectioned constructs.

- Cellularity and GAG content

At the selected time-points of the chondrogenic model (10 and 20 culture days), the culture medium was removed, and the samples were stored at −80 °C for quantitative assays using polypropylene tubes containing a sterile enzymatic solution. The digestive solution consisted of proteinase K, pepstatin A and iodoacetamide dissolved in EDTA. Cell lysates were obtained using freeze-thaw cycles each, namely, quench in liquid N_2, defrosting at 37 °C followed by vortexing. Each cycle had the duration of 30 min and was repeated three times. Following this procedure, the contents of double stranded (ds)-DNA and GAGs could be thus quantified in cascade on the same specimens ($n = 3$). Ds-DNA content in cellular lysates was measured using the PicoGreen assay, as previously reported [43]. Briefly, working buffer and PicoGreen dye solution were prepared according to the manufacturer's instructions using reagents provided within the kit. After 10 min of incubation in the dark at room temperature, the fluorescence intensity of the samples was measured on a plate reader (Victor3; PerkinElmer, Waltham, MA, USA), using an

excitation wavelength of 485 nm and an emission wavelength of 535 nm. To determine the GAG content, the samples immersed in their residual lysates were processed for the enzymatic digestion, which was carried out inside a water bath for 16 h at 60 °C. Thereafter, the DMMB assay was performed, as previously reported [43]. Absorbance was measured at 520 nm using a plate spectrophotometer (Bio-Rad Laboratories, Hercules, CA, USA). Results were expressed as the ratio between GAG content and ds-DNA content at 10 and 20 culture days. Values were then analyzed by statistical analysis.

2.10. Epithelial Cytokine Evaluation

The immunomodulatory properties of the scaffolds (1.5 mm thickness) were studied on skin keratinocytes HaCaT via Real Time PCR, using the primers and parameters reported in Table 1.

Table 1. Analyzed genes involved in the immune response of HaCaT cells seeded on PVA/G sponges.

Gene	Primers Sequence	Conditions	Base Pairs
IL-1α	5′-CATGTCAAATTTCACTGCTTCATCC -3′ 5′-GTCTCTGAATCAGAAATCCTTCTATC -3′	5 s at 95 °C, 8 s at 55 °C, 1 s at 72 °C for 45 cycles	421
IL-1β	5′-GCATCCAGCTACGAATCTCC-3′ 5′-CCACATTCAGCACAGGACTC-3′	5 s at 95 °C, 14 s at 58 °C, 28 s at 72 °C for 40 cycles	708
TNF-α	5′-CAGAGGGAAGAGTTCCCCAG -3′ 5′-CCTTGGTCTGGTAGGAGACG -3′	5 s at 95 °C, 6 s at 57 °C, 13 s at 72 °C for 40 cycles	324
IL-6	5′-ATGAACTCCTTCTCCACAAGCGC-3′ 5′-GAAGAGCCCTCAGGCTGGACTG-3′	5 s at 95 °C, 13 s at 56 °C, 25 s at 72 °C for 40 cycles	628
IL-8	5-ATGACTTCCAAGCTGGCCGTG -3′ 5-TGAATTCTCAGCCCTCTTCAAAAACTTCTC-3′	5 s at 94 °C, 6 s at 55 °C, 12 s at 72 °C for 40 cycles	297
TGF-β	5′-CCGACTACTACGCCAAGGAGGTCAC-3′ 5′-AGGCCGGTTCATGCCATGAATGGTG-3′	5 s at 94 °C, 9 s at 60 °C, 18 s at 72 °C for 40 cycles	439
hBD-2	5′-GGATCCATGGGTATAGGCGATCCTGTTA-3′ 5′-AAGCTTCTCTGATGAGGGAGCCCTTTCT-3′	5 s at 94 °C, 6 s at 63 °C, 10 s at 72 °C for 50 cycles	198

Immortalized human keratinocyte HaCaT cell line was expanded in DMEM-HG supplemented with 1% Penstrep, 1% glutamine and 10% fetal calf serum at 37 °C in air and 5% CO_2. When 80% confluence was reached, 2×10^6 cells resuspended in 50 μL of DMEM were seeded on sponges of 70/30 (*w*/w%) PVA/G placed in 96-well plates. After 4 h from seeding, 100 μL of DMEM were added to the wells and incubated for 24 h. The same number of cells was seeded in a control well without the sponges. To verify the anti-inflammatory activity of the tested sponges, some wells were treated with lipopolysaccharide (LPS) of *Pseudomonas aeruginosa* and lipoteichoic acid (LTA) of *Staphylococcus aureus* (both at concentration of 10 μg/mL), for additional 24 h. A cell seeded well, in which no inflammatory molecule was added, was intended as untreated control. At the endpoint, total RNA was isolated with Tri-Reagent and 1 μg was reverse-transcribed into complementary DNA (cDNA) using random hexamer primers, at 42 °C for 45 min, according to the manufacturer's instructions. Real time PCR was carried out with the LC Fast Start DNA Master SYBR Green kit using 2 μL of cDNA, corresponding to 10 ng of total RNA in a 20 μL final volume, 3 mM $MgCl_2$ and 0.5 μM sense and antisense primers. Real-Time PCR were carried out in order to evaluate the expression of IL-1α, IL-1β, TNF-α, IL-6 and IL-8, TGF-β and hBD-2 (Table 1).

2.11. Statistical Analysis

Statistical analysis was carried out using Student's t-test. The analysis was conducted by comparing the data of independent experiments and the differences were considered statistically significant for $p < 0.05$. Data are expressed as mean $\pm$ standard deviation.

3. Results

3.1. Chatacterization of PVA/G Spongy Scaffolds

In this study, PVA/G sponges were produced to be tested as scaffolds for nasal tissue regeneration. In particular, starting from a PVA water solution and G, we fabricated PVA/G scaffolds at two weight compositions, i.e., 80/20 (*w*/w%) and 70/30 (*w*/w%), using the emulsion and freeze drying method followed by GTA vapor cross-linking. After production, the sponges underwent morphological and physico-mechanical characterization. The results of morphological evaluation are shown in Figure 1. Specifically, both lyophilized sponges showed a highly porous structure, with rounded pores, covering a wide range of diameters, that appeared to be interconnected, as displayed by SEM (Figure 1a,b). A representative surface analysis of these sponges performed using AFM is shown in Figure 1c. This technique highlighted the 3D spongious architecture, showing quite smooth poral surfaces. The results of microCT analysis confirmed the extremely porous character of the sponges (Figure 1d). Specifically, the volume porosity and the pore interconnectivity percentages were 84.43% and 97.44%, respectively, the latter calculated using a cut-off of 4 voxels (corresponding to 51.2 μm pore-pore openings).
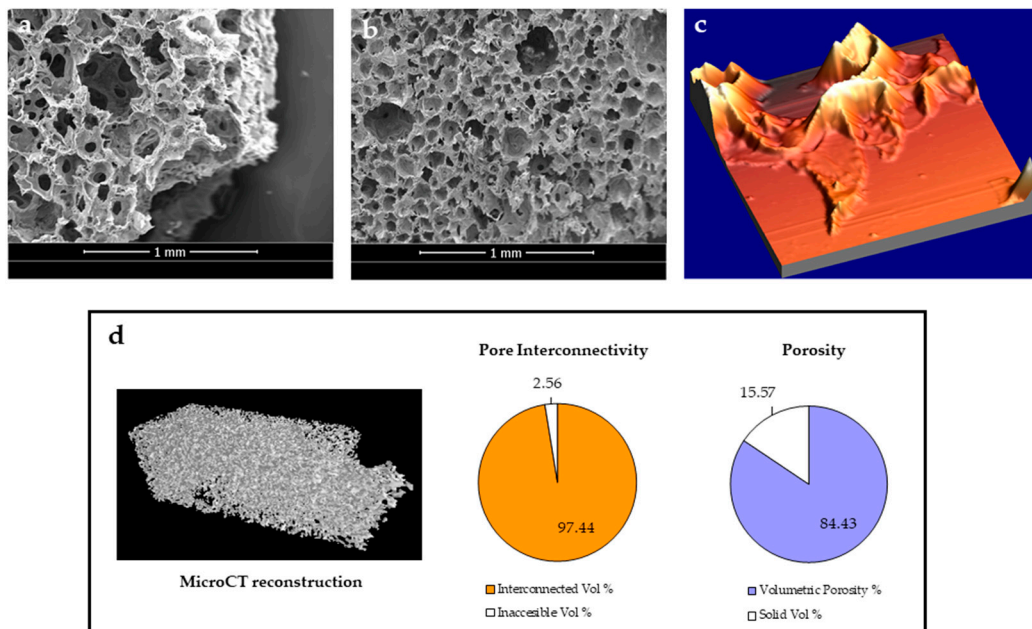

Figure 1. Results of morphological analysis of PVA/G sponges, showing: (**a**,**b**) SEM micrographs of 80/20 and 70/30 (*w*/w%) compositions, respectively, taken at 100× magnification and 15 kV; (**c**) AFM image displaying the PVA/G 80/20 (*w*/w%) sponge inner topography in 40 × 40 μm^2 (1024 × 1024 pixel) area; (**d**) the results of microCT analysis, including a 3D reconstruction of the PVA/G 80/20 (*w*/w%) sponge, the calculated percentages of volumetric pore interconnectivity and porosity.

PVA/G sponges were highly hydrophilic, as water absorption caused a fast swelling (Figure 2a); moreover, they can be squeezed and recover their initial shape (Supplementary video S1). The volume swelling ratio Q was 2.30 ± 0.75 and 1.98 ± 0.09 for PVA/G 80/20 and 70/30 (*w*/w%), respectively, with no statistically significant difference between the two (p = n.s.) (Figure 2b). The wet sponges were used for compressive mechanical tests, which revealed the soft nature of these materials. In fact, 0.69 ± 0.04 kPa were necessary to produce 50% strain under compression in PVA/G 80/20 (*w*/w%) sponges (Figure 2c).
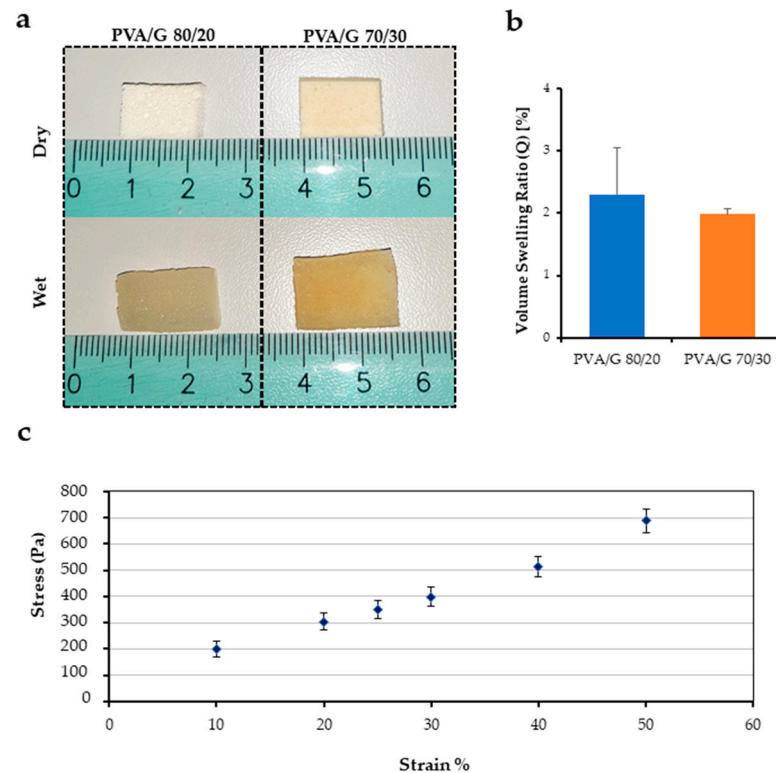
Figure 2. Results of physico-mechanical analysis of PVA/G sponges: (**a**) photograph of PVA/G 80/20 and PVA/G 70/30 (*w*/w%) sponges dry and wet; (**b**) bar graph showing the volume swelling ratio for PVA/G 80/20 and 70/30 (*w*/w%); (**c**) point graph displaying the mechanical behavior of wet PVA/G 80/20 (*w*/w%) sponge under compression.

3.2. Set-Up and Characterization of 3D Nasal Tissue Models

3.2.1. Cartilage Regeneration

PVA/G scaffolds were used to generate a 3D cartilage model by culturing chondrodifferentiated rMSCs in PVA/G 80/20 (*w*/w%) scaffolds. The results of histological analysis are shown in Figure 3, and for scaffold-less controls in Figure S1. H&E staining showed that the scaffolds were well colonized by chondro-differentiated cells and that many clusters of rounded cells were present in the scaffold pores, as also clearly shown by SEM, even though elongated cells were also detected (Figure 3a,b). Alcian blue staining at pH 1 revealed the presence of sulphated acidic GAGs typical of cartilage tissue (Figure 3c). In addition, IHC analysis highlighted a good immunopositivity for the cartilaginous markers Sox-9 and Aggrecan, and a strong immunopositivity for Collagen type II (Figure 3d,f). Quantitative data to support chondrogenic differentiation and immunopositivity are reported in Figure 4. GAG content normalized by sample cellularity resulted significantly higher in the constructs chondro-differentiated for 20 days than in those chondro-differentiated for 10 days, being GAGs/ds-DNA ratio at 10 and 20 culture days: 2.05 ± 0.12 and 2.62 ± 0.48, respectively; $p < 0.01$ (Figure 4a). The number of rounded cells was instead significantly higher at 10 days than at 20 days, being 434 ± 146 and 260 ± 135, respectively, $p < 0.01$) (Figure 4b). However, the number of grouped rounded cells (i.e., forming clusters) at 20 days was superior to the total number of rounded cells, as quantified by the RCG/RTC ratio at 10 and 20 days, which was 0.02 ± 0.01 and 0.03 ± 0.02, respectively, $p < 0.05$) (Figure 4c).
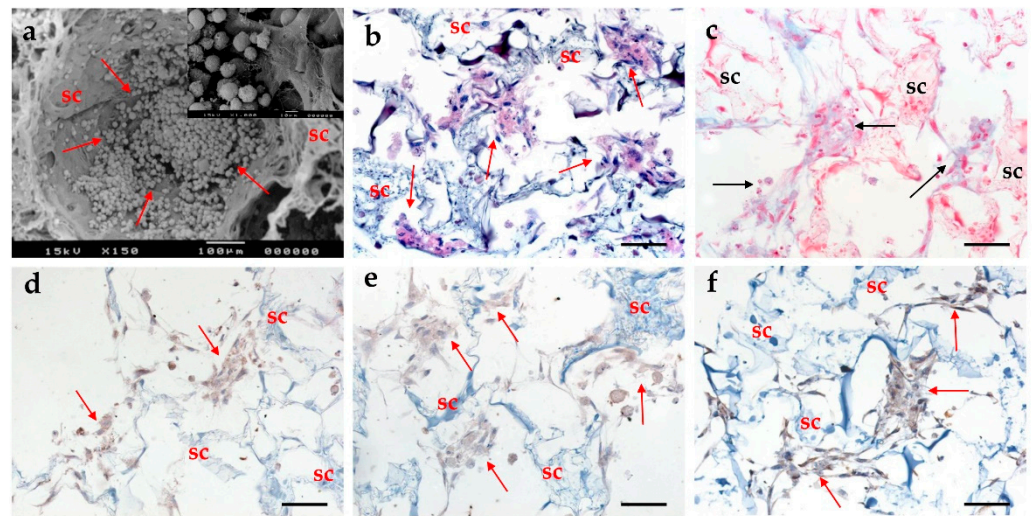
Figure 3. Morphological and histological analysis of the 3D cartilage model (10 differentiation days): (**a**) SEM micrograph showing round-shaped cells in a large pore of the scaffold. Lens shows the morphology of rounded cells; (**b**) H & E staining: cell nuclei are in blue-violet, cytoplasm is in pink; (**c**) Alcian blue pH 1 staining: sulphated GAGs are in cyan, cell nuclei are in red; (**d**–**f**) IHC analysis for: (**d**) Sox-9, (**e**) aggrecan, (**f**) collagen type II. Antigen expression is in brown, cell nuclei are in blue-violet. Sc = scaffold; red arrows = cells. (**b**–**f**) Scale bar = 50 μm. Original magnification 400×.
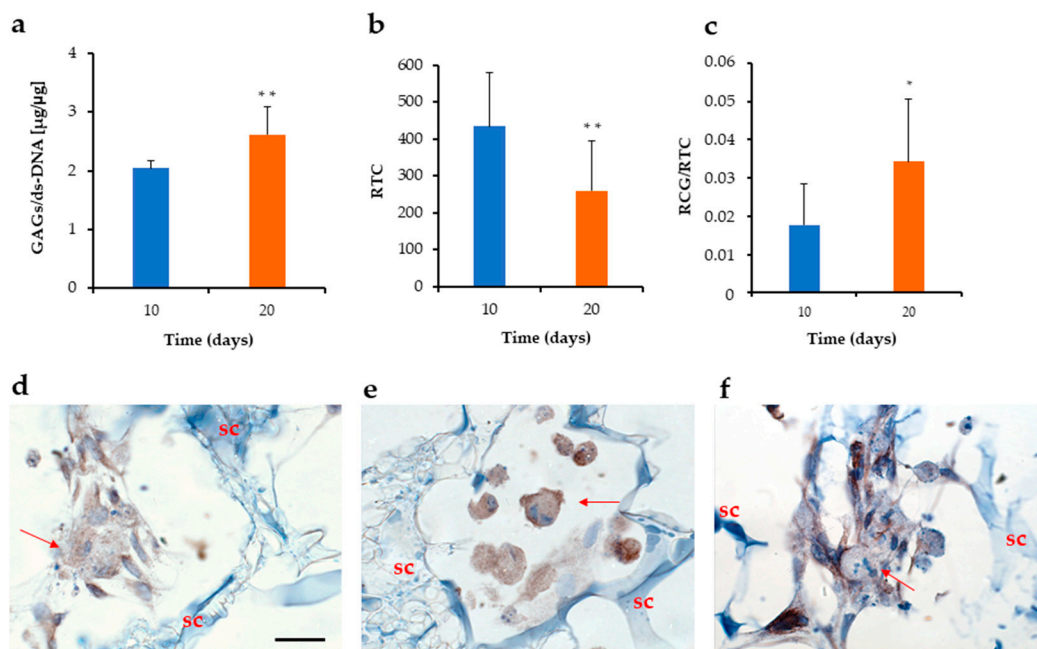

Figure 4. Bar graphs of the 3D cartilage model at 10 and 20 differentiation days: (**a**) GAG content normalized by ds-DNA content; (**b**) RTC number evaluated at 10 and 20 days; (**c**) RCG number normalized by RTC evaluated at 10 and 20 days. * $p < 0.05$; ** $p < 0.01$. RTC = Rounded Total Cells; RCG = Rounded Cell Groups. (**d**–**f**) Immunohistochemistry for Sox-9, Aggrecan and collagen type II in brown, showing cell groups. Arrows point to examples of viable cell nuclei. Scale bar = 20 μm. Original magnification 1000×.

3.2.2. Prevascularized Bone Regeneration

The histological analysis of a 3D osteogenic model incorporating pre-endothelial cells, both deriving from MPCs, inside PVA/G 80/20 (*w*/w%) scaffolds is reported in Figure 5. IHC analysis showed immunopositivity for two key osteogenic markers, i.e., ALP and Osteocalcin (Figure 5a,b). Von Kossa staining revealed in black a large amount of mineral-

ized matrix surrounding the pores of the scaffolds (Figure 4c). Concerning the endothelial markers, IHC showed a strong positivity for Flk-1 (Figure 5d). Differently, p-Klk-1 and PECAM-1 were immunonegative (Figure 5e,f).
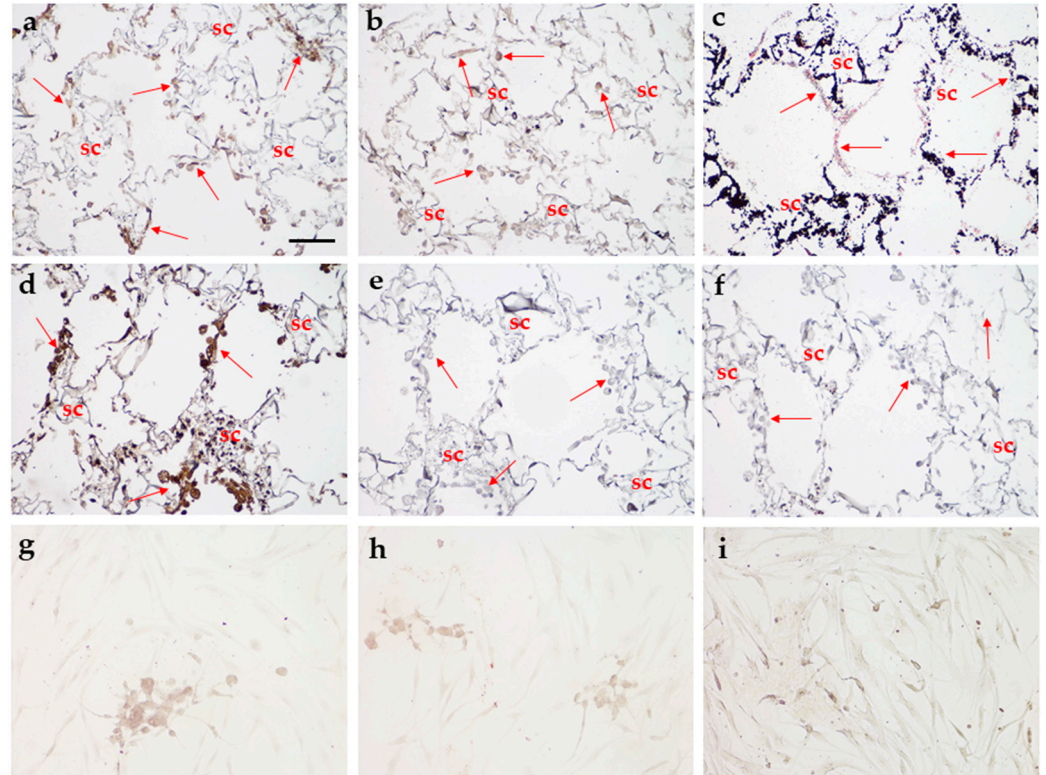

Figure 5. Histological analysis of the 3D osteogenic model and MPCs endothelial differentiation in 2D culture. (**a**–**f**) Osteogenic model: (**a**) IHC analysis for ALP; (**b**) IHC analysis for Osteocalcin; (**c**) von Kossa staining: mineralized matrix in black, cell nuclei in red; (**d**) IHC analysis for Flk-1; (**e**) IHC analysis for p-Flk-1; (**f**) IHC analysis for PECAM-1. (**g**–**i**) Endothelial differentiation of MPCs in 2D model: IHC analysis for: (**g**) Flk-1, (**h**) p-Flk-1, (**i**) PECAM-1. SEM analysis. Antigen expression is revealed in brown, cell nuclei are in blue-violet. Sc = scaffold; red arrows = cells. Scale bar = 100 μm. Original magnification 200×.

MPCs terminally differentiated towards endothelial lineage in 2D, as demonstrated in chamber slide culture, where they were immunopositive for both Flk-1 and p-Flk-1 only in some cells, and weakly immunopositive for PECAM-1 (Figure 5g–i).

3.2.3. Fibrocartilage Regeneration

The outcomes of a 3D fibrocartilage model grown by differentiating hMSCs inside PVA/G 70/30 (*w*/w%) scaffolds are presented in Figure 6. H & E staining highlighted that the differentiated hMSCs were able to colonize the entire scaffold pores, by also secreting ECM in large amount in the whole scaffold (Figure 6a). Alcian Blue staining at pH 1 revealed sulphated acidic GAGs (Figure 6b). IHC analysis was negative for Aggrecan and Collagen type II, but detected strong immunopositivity for Sox-9 and Collagen type I (Figure 6c–f).
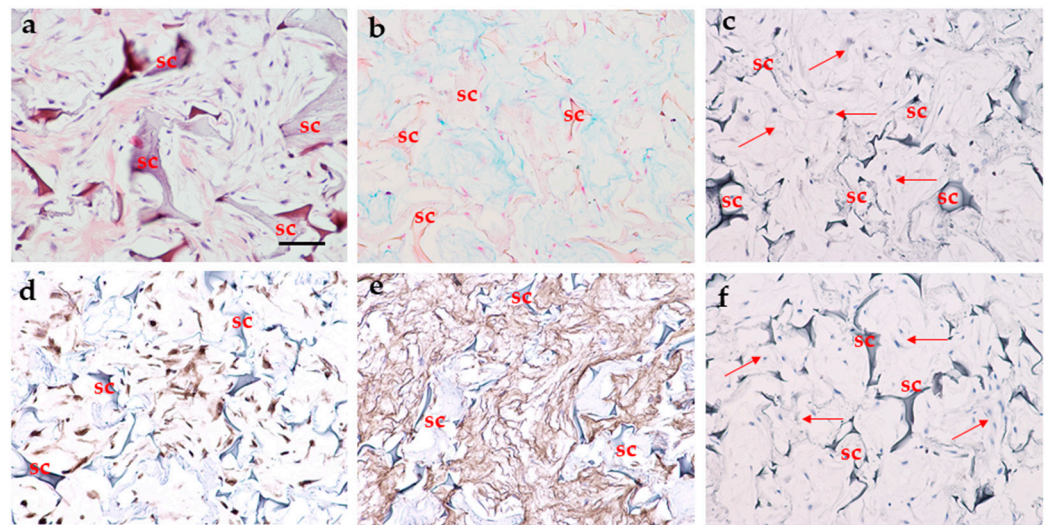
Figure 6. Histological analysis of the 3D fibrocartilage model. (**a**) H & E staining: cell nuclei are in blue-violet, cytoplasm is in pink; (**b**) Alcian blue pH1 staining: sulphated GAGs are in cyan, cell nuclei are in red; (**c**–**f**) IHC analysis for: (**c**) aggrecan (**d**) Sox-9, (**e**) collagen type I, (**f**) collagen type II. Antigen expression is revealed in brown, cell nuclei are in blue-violet. Sc = scaffold; red arrows = cells. (**b**–**f**) Scale bar = 100 μm. Original magnification 200×.

3.3. Immuno-Modulatory Activity of Keratinocytes towards PVA/G SCAFFOLDs

RT-PCR analysis for pro-inflammatory cytokines and antimicrobial molecules was performed after growing HaCaT cells onto PVA/G 70/30 (*w*/w%) scaffolds, and the obtained results are given in Figure 7.
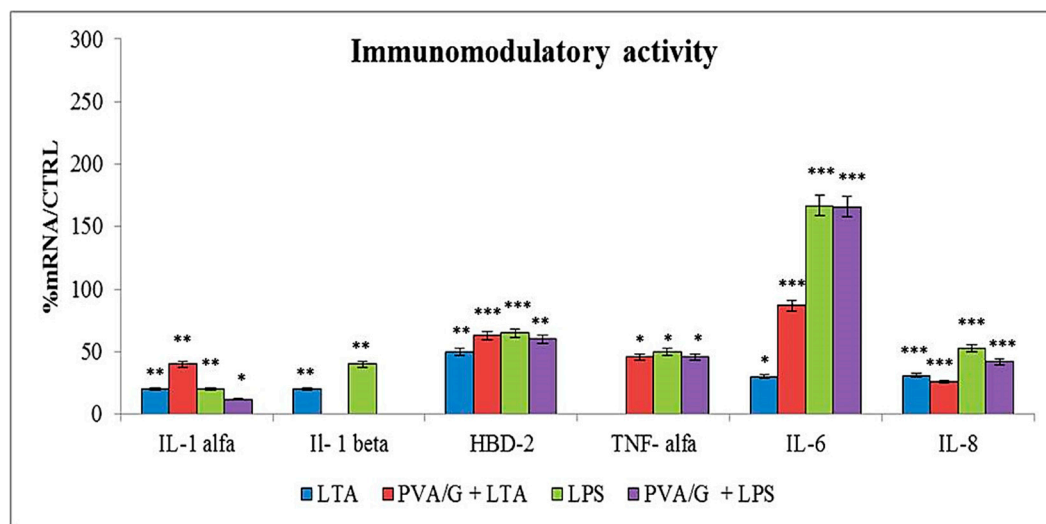

Figure 7. Bar graph reporting the RT-PCR results related to the HaCaT cell response to PVA/G scaffold. mRNA expression was normalized for the basal expression of untreated HaCaT cells. PVA/G = Poly(vinyl alcohol)/Gelatin; LTA = lipoteichoic acid; LPS = lipopolysaccharide; IL = interleukin; TNF = tumor necrosis factor; HBD-2 = human beta defensin 2. Data are expressed as mean ± SD versus cells cultured without biomaterials; * $p < 0.05$; ** $p < 0.01$; *** $p < 0.001$.

The effect of the scaffold on HaCaT cells was evaluated in the presence of LPS or LTA, as pro-inflammatory molecules. The presence of the sponge slightly changed the overall gene expression profile of the investigated cytokines, confirming that the scaffold is neither significantly promoting inflammatory processes, nor interfering with the production of hBD2. Interestingly, in presence of the scaffold, IL-1β was not upregulated by LPS or LTA.

4. Discussion

The nose is a complex organ consisting of several tissue types that are mechanically and functionally interconnected with each other to prime the respiratory function: cartilaginous, bony, epithelial, adipose and fibromuscular tissues, among others. The shape and integrity of all the nasal tissues are fundamental for its physiology. Due to its exposed position, the nose is affected by several pathologies, mainly derived from allergy, infections, traumas, burns, chemical agents, drugs, and tumors [1–4]. In particular, tumor resection leads to deformation of the nasal structures with impairment of its function and aesthetics, thus necessitating reconstructive surgery, which is expensive and complex, as it requires several interventions. Due to its specific function and location, and for environmental factors like air pollution, the nose is challenged by inflammatory processes. Therefore, novel biomaterial approaches able to provide safe repair and reconstruction are greatly needed. Having a biomaterial suitable for reconstructing different nasal tissues would offer a better versatile platform for rhinoplasty.

Recently, the problem of nasal tissue regeneration has been addressed from a TE point of view. In recent decades, the TE paradigm, comprising cells, 3D biomaterial scaffolds and appropriate stimuli, has been explored in many medical fields, including nose reconstruction, albeit in limited studies. Although good results have been obtained, recently also in humans, no TE construct has yet been found to regenerate damaged nose in all its components [28].

Starting from these assumptions, we generated in vitro constructs made of PVA/G scaffolds and stem cells differentiated towards different lineages and we performed a morpho-functional investigation to assess potential to obtain cartilage tissue for repairing septum and lateral cartilages, bone tissue for the vomer and other bone structures, fibrous tissue for the regeneration of the connective ligaments and alae. PVA is a very versatile and widely known biocompatible material, used in many TE studies, but not yet evaluated for nasal structures [44]. G is a natural protein obtained from collagen denaturation. As the denaturation process preserves many functional groups of native collagen, G is able to interact with cells and facilitate their adhesion [45]. Moreover, we demonstrated that the addition of G during the emulsion process helps the foam porogenesis, which ultimately leads to pore size distribution in the range of cellular size [35]. Overall, G affects pore formation, size and interconnectivity via foaming, is responsible for sponge stability via GTA crosslinking, and modulates the surface properties of PVA to trigger cell adhesion. Considering our previous studies on PVA/G sponges, we observed that G within 20–30% by weight with respect to PVA led to sponges suitable for the growth of several cell types [30,34,35,40]. In fact, as we showed here, both 80/20 and 70/30 (w/w%) PVA/G sponges displayed a highly porous architecture, with round-shaped pores and quite smooth surfaces. The sponges demonstrated a volumetric porosity of ~ 85% and pore interconnectivity of ~97%, measured by considering minimum pore-pore openings of 52 μm. This evidence indicates that only ~3% of the scaffold volume is either inaccessible or connected through lower size openings, which, however, can contribute to oxygen and nutrient diffusion across the scaffold. Upon wetting, both sponge types almost doubled their volume, ultimately reaching a water content similar to that of cartilage [29]. Wet sponges were extremely soft in nature, as corroborated by compressive mechanical tests, and were provided with shape recovery, which is a remarkable feature for minimally invasive surgery. Both formulations thus showed very similar behavior, which was considered to fit nasal applications.

In addition to providing a scaffold suitable for diverse nasal tissues, the second key point of this study was to suggest a unique cell source for regenerating those tissues, and in particular, cartilage, pre-vascularized bone and fibrous tissue. We thus proposed the use of MPCs isolated from the human bone marrow, as they are able to give rise to pre-endothelial cells and to MSCs, the latter capable of differentiating into several mesodermal lineages [37,38,41]. In a previous work, we tested PVA/G scaffolds for the regeneration auricle cartilage, finding that it was promising for elastic cartilage engineering [34]. In fact, we obtained elastic fibers by applying mechanical forces during the chondrogenic differen-

tiation of MSCs. In this study, rMSCs seeded on the PVA/G sponges were differentiated towards the chondrogenic phenotype aimed to obtain a hyaline cartilage model. MSCs proliferated and chondro-differentiated efficiently in PVA/G scaffolds. The obtained results showed that the cells colonized the scaffold also in depth. Moreover, differently from other cell sources, like dental pulp [43], the bone marrow MSCs in this scaffold massively assumed a rounded morphology and acquired the ability to aggregate into clusters within its pores already after 10 days, but mainly after 20 days of chondrogenic differentiation. Differentiated MSCs also gave rise to the production of molecules typical of hyaline cartilage, such as sulphated acidic GAGs and collagen type II. As aggregation into isogenic groups is a hallmark of hyaline cartilage, the positivity to these specific chondrogenic markers indicates that this scaffold is advantageous to support chondrogenic differentiation of bone marrow MSCs [46]. We thereafter used hMSCs to generate a panel of 3D nasal tissue models. Unlike cartilage, bone is vascularized tissue. The key steps towards optimized clinical applications of tissue-engineered bone substitutes rely on neovascularization of the engineered construct after implantation [47]. For this reason, strategies enabling subsequent in vivo vasculogenesis, such as the addition of vascular endothelial cells are being investigated [35]. In the pre-vascularized osteogenic model, we aimed to exploit the angiogenetic and osteogenic potential of a specific subpopulation of bone marrow cells, recently known as MPCs. In parallel cultures, MPCs were differentiated either into pre-endothelial cells or into MSCs, the latter further seeded on the scaffolds upon osteogenic differentiation. The pre-endothelial cells differentiated in 2D culture were then seeded on the 3D bone model generated in the meantime for a final coculture step, as similarly reported in a previous study [35]. In the obtained construct, the production of bone ECM and the expression of osteogenic markers, such as ALP and OCN, along with the strong immunopositivity for the VEGF receptor Flk-1 highlighted in some cells, suggested that the PVA/G scaffold allowed both osteogenic and endothelial differentiation of MPCs. This evidence is confirmed by the comparison with MPCs differentiated in 2D culture, in which this protein was poorly expressed. On the other hand, PECAM and the phosphorylated form of the Flk-1 receptor, weakly expressed in the 2D culture, were absent in our 3D model, indicating the need to further investigate the role of the PVA/G sponge in the endothelial differentiation of MPCs, due to their early angiogenic potential [38]. This pre-vascularized bone model retraced the findings previously obtained using hUVECs and hMSCs by instead using a single cell source, patient-derived, which better opens up translational perspectives [35].

PVA/G sponges are mechanically soft materials, although the addition of G is able to increase the sponge elastic modulus by virtue of the chemical crosslinking [34,48]. In general, for PVA scaffolds, a low mechanical strength has been reported, which may not be suitable for skeletal bone engineering [49]. Conversely, as a part of the facial bones, the nasal bone is not subjected to mechanical loading, so other characteristics, such as high porosity, large pore size and water absorption capacity could play a relevant role in this context. Most importantly, a material that allows tissue continuity between the different structural parts of the nose is needed. In fact, the bone ECM secreted by the cells could finally provide the necessary mechanical strength proper of bone. The hMSCs obtained from the MPCs were finally used to generate a 3D model of fibrocartilage. By tuning the differentiative stimuli in the culture, we selected an intermediate cell population producing massive amount of collagen type I but still retaining some chondrogenic characteristics, as shown by the production of sulphated acidic GAGs and by the immunopositivity for the transcription factor Sox-9. Our fibrocartilage tissue model is representative of the connective tissue that builds up the ligaments connecting the nose anatomical structures, the alar tissue, and that anchors the nose to the facial bones [39]. All in all, we showed that PVA/G sponges and a single cell source, i.e., the MPCs, have a wide potential for the regeneration of nasal tissues, which could be tuned by varying the culture conditions (i.e., biochemical stimuli). Possessing several features on different length scales, such as properly distributed pore sizes showing surfaces of suitable roughness [50,51], along with

befitting chemical moieties provided by a natural biopolymer in proper concentration, PVA/G scaffolds allowed the regeneration of several mesodermal tissues, including zonal transition tissue, which are greatly important in TE applications [52].

As a first defense line for our breathing organs, the nose is naturally exposed to pathogens, including viruses, fungi and bacteria, which interact with the nasal epithelium. To respond pathogenic insults, our epithelia can secrete pro-inflammatory cytokines that trigger immune response, as well as antimicrobial peptides as for innate immunity [53]. A recurrently inflamed or infected microenvironment challenges the presence of biomaterials implanted in the human body, leading to extrusion phenomena when synthetic non-bioresorbable materials are used. At the end of the nose surgery, de-epithelialized areas of the nasal septum or fossa need to be protected to avoid bacterial infiltration and biofilm formation [54]. We thus explored whether PVA/G scaffolds could interfere with the immunomodulatory response performed by epithelial cells. Immortalized human keratinocyte, HaCaT cells, were put in contact with PVA/G sponges and incubated with two types of molecules produced by bacteria, and thus were able to promote inflammatory processes led by epithelial cells: LPS from *Pseudomonas aeruginosa* and LTA from *Staphylococcus aureus*. Gene expression of the pro-inflammatory cytokines involved in the immune response was evaluated by comparing the HaCaT cells growth in contact with PVA/G scaffolds and alone. Our findings showed a similar behavior between these two culture conditions, thus suggesting that PVA/G scaffolds should not significantly affect the epithelial inflammatory response toward microbial agents. Moreover, the presence of G in combination with synthetic polymers can enhance the overall biocompatibility, as also demonstrated by previous studies [55,56].

Having a simple scaffold/stem cell platform for the regeneration of several nasal tissues would promote better satisfactory esthetic and functional outcomes in rhinoplasty, including reconstruction after sinonasal tumor surgery.

5. Conclusions

Regenerating diverse nasal tissues to be implanted via minimally invasive surgery represents a challenge. Our study showed that it is possible to obtain different 3D constructs for the regeneration of full thickness nasal damage, using a single cell population (i.e., MPCs) and only one type of scaffold (i.e., PVA/G sponges with G at 20–30% w/w). We could efficiently perform chondrogenic, fibroblastic, osteogenic and vasculogenic differentiation using stem cells in vitro on PVA/G scaffolds. Moreover, we proved that the sponges did not increase inflammatory cytokine expression by human dermal keratinocytes in presence of inflammatory insults. Overall, for their cytocompatibility with connective and epithelial tissues, soft nature and shape recovery capacity, which helps the surgical insertion, PVA/G sponges offer a flexible option in nose tissue engineering.

Further studies will be needed to test the effective regenerative capability in vivo of these scaffolds, their long-term performance and biocompatibility, including interactions with pathogens. However, obtaining these constructs could represent an interesting step forward in the repairing of the injuries affecting the different anatomical structures of the nose.

Author Contributions: Conceptualization, S.D., D.D. and M.P.; methodology, L.P.S., G.D., M.P., L.T.; validation, S.M., A.F., L.T.; formal analysis, S.D. and D.D.; investigation, S.M., A.F., J.G.D.l.O., L.T., M.F., M.D.; resources, M.D., G.D., M.P., S.B. and S.D.; data curation, D.D.; writing—original draft preparation, D.D.; writing—review and editing, S.D..; visualization, S.D.; supervision, S.D.; project administration, S.D.; funding acquisition, S.B. and S.D. All authors have read and agreed to the published version of the manuscript.

References

1. Harkema, J.R.; Carey, S.A.; Wagner, J.G. The nose revisited: A brief review of the comparative structure, function, and toxicologic pathology of the nasal epithelium. *Toxicol. Pathol.* **2006**, *34*, 252–269. [CrossRef] [PubMed]
2. Lavernia, L.; Brown, W.E.; Wong, B.J.F.; Hu, J.C.; Athanasiou, K.A. Toward tissue-engineering of nasal cartilages. *Acta Biomater.* **2019**, *88*, 42–56. [CrossRef] [PubMed]
3. Jankowski, R.; Rumeau, C.; de Saint Hilare, T.; Tonnelet, R.; Nguyen, D.T.; Gallet, P.; Perez, M. The olfactory fascia: An evo–devo concept of the fibrocartilaginous nose. *Surg. Radiol. Anat.* **2016**, *38*, 1161–1168. [CrossRef] [PubMed]
4. Rajzer, I.; Stręk, P.; Wiatr, M.; Skladzien, J.; Kurowska, A.; Kopeć, J.; Swiezy, K.; Wiatr, A. Biomaterials in the reconstruction of nasal septum perforation. *Ann. Otol. Rhinol. Laryngol.* **2020**. Online ahead of print. [CrossRef] [PubMed]
5. Popko, M.; Bleys, R.L.A.W.; de Groot, J.W.; Huizing, E.H. Histological structure of the nasal cartilages and their perichondrial envelope. I. The septal and lobular cartilage. *Rhinol. Int. J.* **2007**, *45*, 148–152.
6. Holden, P.K.; Liaw, L.; Wong, B.J.F. Human nasal cartilage ultrastructure: Characteristics and comparison using scanning electron microscopy. *Laryngoscope* **2008**, *118*, 1153–1156. [CrossRef]
7. Saban, Y.; Amodeo, C.A.; Hammou, J.C.; Polselli, R. An anatomical study of the nasal superficial musculoaponeurotic system surgical applications in rhinoplasty. *Arch. Facial Plast. Surg.* **2008**, *10*, 109–115. [CrossRef]
8. Park, J.; Suhk, J.; Nguyen, A.H. Nasal analysis and anatomy: Anthropometric proportional assessment in asians-aesthetic balance from forehead to Chin, Part II. *Semin. Plast. Surg.* **2015**, *29*, 226–231. [CrossRef]
9. Ozturk, C.N.; Larson, J.D.; Ozturk, C.; Zins, J.E. The SMAS and fat compartments of the nose: An anatomical study. *Aesthetic Plast. Surg.* **2013**, *37*, 11–15. [CrossRef]
10. Roblin, D.G.; Eccles, R. What, if any, is the value of septal surgery? *Clin. Otolaryngol. Allied Sci.* **2002**, *27*, 77–80. [CrossRef]
11. Andrews, S.H.J.; Kunze, M.; Mulet-Sierra, A.; Williams, L.; Ansari, K.; Osswald, M.; Adesida, A.B. Strategies to mitigate variability in engineering human nasal cartilage. *Sci. Rep.* **2017**, *7*, 6490. [CrossRef]
12. Pirsig, W.; Kern, E.B.; Verse, T. Reconstruction of anterior nasal septum: Backto-back autogenous ear cartilage graft. *Laryngoscope* **2004**, *114*, 627–638. [CrossRef] [PubMed]
13. Bussi, M.; Palonta, F.; Toma, S. Grafting in revision rhinoplasty. *Acta Otorhinolaryngol. Ital.* **2013**, *33*, 183–189.
14. Kim, J.H.; Song, J.W.; Park, S.W.; Oh, W.S.; Lee, J.H. 10th Rib cartilage: Another option of the costal cartilage graft for rhinoplasty. *Arch. Aesthetic Plast. Surg.* **2015**, *21*, 47–53. [CrossRef]
15. Revell, C.M.; Athanasiou, K.A. Success rates and immunologic responses of autogenic, allogenic, and xenogenic treatments to repair articular cartilage defects. *Tissue Eng. Part B Rev.* **2009**, *15*, 1–15. [CrossRef] [PubMed]
16. Huizing, E.H.; Mackay, I.S.; Rettinger, G. Reconstruction of the nasal septum and dorsum by cartilage transplants–autogeneic or allogeneic? *Rhinology* **1989**, *27*, 5–10. [PubMed]
17. Patel, K.; Brandstetter, K. Solid implants in facial plastic surgery: Potential complications and how to prevent them. *Facial Plast. Surg.* **2016**, *32*, 520–531. [PubMed]
18. Stelter, K.; Strieth, S.; Berghaus, A. Porous polyethylene implants in revision rhinoplasty: Chances and risks. *Rhinology* **2007**, *45*, 325–331. [PubMed]
19. Graham, M.E.; Gratzer, P.F.; Bezuhly, M.; Hong, P. Development and characterization of decellularized human nasoseptal cartilage matrix for use in tissue engineering. *Laryngoscope* **2016**, *126*, 2226–2231. [CrossRef]
20. Schwarz, S.; Elsaesser, A.F.; Koerber, L.; Goldberg-Bockhorn, E.; Seitz, A.M.; Bermueller, C.; Durselen, L.; Ignatius, A.; Breiter, R.; Rotter, N. Processed xenogenic cartilage as innovative biomatrix for cartilage tissue engineering: Effects on chondrocyte differentiation and function. *J. Tissue Eng. Regen. Med.* **2015**, *9*, E239–E251. [CrossRef]
21. Kundu, J.; Shim, J.H.; Jang, J.; Kim, S.W.; Cho, D.W. An additive manufacturing based PCL-alginate-chondrocyte bioprinted scaffold for cartilage tissue engineering. *J. Tissue Eng. Regen. Med.* **2015**, *9*, 1286–1297. [CrossRef]

22. Hoshi, K.; Fujihara, Y.; Saijo, H.; Asawa, Y.; Nishizawa, S.; Kanazawa, S.; Uto, S.; Inaki, R.; Matsuyama, M.; Sakamoto, T.; et al. Implant-type tissue-engineered cartilage for secondary correction of cleft lip-nose patients: An exploratory first-in-human trial. *J. Clin. Trials* **2017**, *7*, 1–9. [CrossRef]

23. Zhang, J.; Liu, L.; Gao, Z.; Li, L.; Feng, X.; Wu, W.; Ma, Q.; Cheng, X.; Chen, F.; Mao, T. Novel approach to engineer implantable nasal alar cartilage employing marrow precursor cell sheet and biodegradable scaffold. *J. Oral Maxillofac. Surg.* **2009**, *67*, 257–264. [CrossRef] [PubMed]

24. Kim, D.H.; Lim, J.Y.; Kim, S.W.; Lee, W.S.; Park, S.H.; Kwon, M.Y.; Park, S.H.; Lim, M.H.; Back, S.A.; Yun, B.G.; et al. Characteristics of nasal septal cartilage-derived progenitor cells during prolonged cultivation. *Otolaryngol. Head Neck Surg. (US)* **2018**, *159*, 774–782. [CrossRef] [PubMed]

25. Ciorba, A.; Martini, A. Tissue engineering and cartilage regeneration for auricular reconstruction. *Int. J. Pediatr. Otorhinolaryngol.* **2006**, *70*, 1507–1515. [CrossRef]

26. Hoshi, K.; Fujihara, Y.; Saijo, H.; Kurabayashi, K.; Suenaga, H.; Asawa, Y.; Nishizawa, S.; Kanazawa, S.; Uto, S.; Inaki, R.; et al. Three-dimensional changes of noses after transplantation of implant-type tissue-engineered cartilage for secondary correction of cleft lip–nose patients. *Regen. Ther.* **2017**, *7*, 72–79. [CrossRef]

27. Xu, Y.; Fan, F.; Kang, N.; Wang, S.; Jianjun, Y.; Wang, H.; Zhang, B. Tissue engineering of human nasal alar cartilage precisely by using three-dimensional printing. *Plast. Reconstr. Surg.* **2015**, *135*, 451–458. [CrossRef] [PubMed]

28. Niermeyer, W.L.; Rodman, C.; Li, M.M.; Chiang, T. Tissue engineering applications in otolaryngology-The state of translation. *Laryngosc. Investig. Otolaryngol.* **2020**, *5*, 630–648. [CrossRef]

29. Pillai, M.M.; Gopinathan, J.; Kumar, R.S.; Kumar, G.S.; Shanthakumari, S.; Sahanand, K.S.; Bhattacharyya, A.; Selvakumar, R. Tissue engineering of human knee meniscus using functionalized and reinforced silk-polyvinyl alcohol composite three-dimensional scaffolds: Understanding the in vitro and in vivo behavior. *J. Biomed. Mater. Res. A* **2018**, *106A*, 1722–1731. [CrossRef] [PubMed]

30. Moscato, S.; Mattii, L.; D'Alessandro, D.; Cascone, M.G.; Lazzeri, L.; Serino, L.P.; Dolfi, A.; Bernardini, N. Interaction of human gingival fibroblasts with PVA/gelatine sponges. *Micron* **2008**, *39*, 569–579. [CrossRef] [PubMed]

31. Moscato, S.; Ronca, F.; Campani, D.; Danti, S. Poly(vinyl alcohol)/gelatin Hydrogels Cultured with HepG2 Cells as a 3D Model of Hepatocellular Carcinoma: A Morphological Study. *J. Funct. Biomater.* **2015**, *6*, 16–32. [CrossRef] [PubMed]

32. Danti, S.; D'Acunto, M.; Trombi, L.; Berrettini, S.; Pietrabissa, A. A micro/nanoscale surface mechanical study on morphofunctional changes in multilineage-differentiated human mesenchymal stem cells. *Macromol. Biosci.* **2007**, *7*, 589–598. [CrossRef]

33. D'Alessandro, D.; Pertici, G.; Moscato, M.; Metelli, M.R.; Danti, S.; Nesti, C.; Berrettini, S.; Petrini, M.; Danti, S. Processing large-diameter poly(L-lactic acid) microfiber mesh/mesenchymal stromal cell constructs via resin embedding: An efficient histologic method. *Biomed. Mater.* **2014**, *9*, 045007. [CrossRef] [PubMed]

34. Feula, M.; Milazzo, M.; Giannone, G.; Azimi, B.; Trombi, L.; Cacopardo, L.; Moscato, S.; Lazzeri, A.; Ahluwalia, A.; Berrettini, S.; et al. Bioartificial sponges for auricular cartilage engineering. In *LNB-Advances in Bionanomaterials II*; Piotto, S., Concilio, S., Sessa, L., Rossi, F., Eds.; Springer: Cham, Switzerland, 2019; pp. 191–209.

35. De la Ossa, J.G.; Trombi, L.; D'Alessandro, D.; Coltelli, M.B.; Serino, L.P.; Pini, R.; Lazzeri, A.; Petrini, M.; Danti, S. Pore size distribution and blend composition affect in vitro prevascularized bone matrix formation on Poly(Vinyl Alcohol)/Gelatin Sponges. *Macromol. Mater. Eng.* **2017**, *302*, 1700300. [CrossRef]

36. Wang, C.; Li, Y.; Yang, M.; Zou, Y.; Liu, H.; Liang, Z.; Yin, Y.; Niu, G.; Yan, Z.; Zhang, B. Efficient Differentiation of Bone Marrow Mesenchymal Stem Cells into Endothelial Cells in Vitro. *Eur. J. Vasc. Endovasc. Surg.* **2018**, *55*, e265. [CrossRef] [PubMed]

37. Fazzi, R.; Pacini, S.; Carnicelli, V.; Trombi, L.; Montali, M.; Lazzarini, E.; Petrini, M. Mesodermal progenitor cells (MPCs) differentiate into mesenchymal stromal cells (MSCs) by activation of Wnt5/calmodulin signalling pathway. *PLoS ONE* **2011**, *6*, e25600. [CrossRef] [PubMed]

38. Montali, M.; Panvini, F.M.; Barachini, S.; Ronca, F.; Carnicelli, V.; Mazzoni, S.; Petrini, I.; Pacini, S. Human adult mesangiogenic progenitor cells reveal an early angiogenic potential, which is lost after mesengenic differentiation. *Stem Cell Res. Ther.* **2017**, *8*, 106. [CrossRef]

39. Armiento, A.R.; Alini, M.; Stoddart, M.J. Articular fibrocartilage-why does hyaline cartilage fail to repair? *Adv. Drug. Deliv. Rev.* **2019**, *146*, 289–305. [CrossRef]

40. Ricci, C.; Danti, S. 3D models of pancreatic ductal adenocarcinoma via tissue engineering. *Methods Mol. Biol.* **2019**, *1882*, 81–95.

41. Petrini, M.; Pacini, S.; Trombi, L.; Fazzi, L.; Montali, M.; Ikehara, S.; Abraham, N.G. Identification and purification of mesodermal progenitor cells from human adult bone marrow. *Stem Cells Dev.* **2009**, *18*, 857–866. [CrossRef]

42. Maniatopoulos, C.; Sodek, J.; Melcher, A.H. Bone formation in vitro by stromal cells obtained from bone marrow of young adult rats. *Cell Tissue Res.* **1988**, *254*, 317–330. [CrossRef] [PubMed]

43. Barachini, S.; Danti, S.; Pacini, S.; D'Alessandro, D.; Carnicelli, V.; Trombi, L.; Moscato, S.; Mannari, C.; Cei, S.; Petrini, M. Plasticity of human dental pulp stromal cells with bioengineering platforms: A versatile tool for regenerative medicine. *Micron* **2014**, *67*, 155–168. [CrossRef] [PubMed]

44. Ng, K.W.; Wanivenhaus, F.; Chen, T.; Hsu, H.C.; Allon, A.A.; Abrams, V.D.; Torzilli, P.A.; Warren, R.F.; Maher, S.A. A novel macroporous polyvinyl alcohol scaffold promotes chondrocyte migration and interface formation in an in vitro cartilage defect model. *Tissue Eng. Part A* **2012**, *18*, 1273–1281. [CrossRef]

45. Davidenko, N.; Schuster, C.F.; Bax, D.V.; Farndale, R.W.; Hamaia, S.; Best, S.M.; Cameron, R.E. Evaluation of cell binding to collagen and gelatin: A study of the effect of 2D and 3D architecture and surface chemistry. *J. Mater. Sci. Mater. Med.* **2016**, *27*, 148. [CrossRef] [PubMed]

46. Thorp, H.; Kim, K.; Kondo, M.; Grainger, D.W.; Okano, T. Fabrication of hyaline-like cartilage constructs using mesenchymal stem cell sheets. *Sci. Rep.* **2020**, *10*, 20869. [CrossRef]

47. Santos, M.I.; Reis, R.L. Vascularization in bone tissue engineering: Physiology, current strategies, major hurdles and future challenges. *Macromol. Biosci.* **2010**, *10*, 12–27. [CrossRef]

48. Karimi, A.; Navidbaksh, M. Mechanical properties of PVA material for tissue engineering applications. *Mater. Technol.* **2014**, *29*, 90–100. [CrossRef]

49. Kamoun, E.A.; Chen, X.; Eldin, M.S.M.; Kenawy, E.R.S. Crosslinked poly(vinyl alcohol) hydrogels for wound dressing applications: A review of remarkably blended polymers. *Arabian J. Chem.* **2015**, *8*, 1–14. [CrossRef]

50. Limongi, T.; Tirinato, L.; Pagliari, F.; Giugni, A.; Allione, M.; Perozziello, G.; Candeloro, P.; Di Fabrizio, E. Fabrication and applications of micro/nanostructured devices for tissue engineering. *Nano-Micro Lett.* **2017**, *9*, 1. [CrossRef]

51. Limongi, T.; Giugni, A.; Tan, H.; Bukhari, E.M.; Torre, B.; Allione, M.; Marini, M.; Tirinato, L.; Das, G.; Moretti, M.; et al. Fabrication, mercury intrusion porosimetry characterization and in vitro qualitative analysis of biocompatibility of various porosities polycaprolactone scaffolds. *J. Tissue Sci. Eng.* **2015**, *6*, 159. [CrossRef]

52. Smith, L.; Xia, Y.; Galatz, L.M.; Genin, G.M.; Thomopoulos, S. Tissue-engineering strategies for the tendon/ligament-to-bone insertion. *Connect. Tissue Res.* **2012**, *53*, 95–105. [CrossRef] [PubMed]

53. Larsen, S.B.; Cowley, C.J.; Fuchs, E. Epithelial cells: Liaisons of immunity. *Curr. Opin. Immunol.* **2020**, *62*, 45–53. [CrossRef] [PubMed]

54. Milazzo, M.; Gallone, G.; Marcello, E.; Mariniello, M.D.; Bruschini, L.; Roy, I.; Danti, S. Biodegradable polymeric micro/nano-structures with intrinsic antifouling/antimicrobial properties: Relevance in damaged skin and other biomedical applications. *J. Funct. Biomater.* **2020**, *11*, 60. [CrossRef]

55. Lazzeri, L.; Cascone, M.G.; Danti, S.; Serino, L.P.; Moscato, S.; Bernardini, N. Gelatine/PLLA sponge-like scaffolds: Morphological and biological characterization. *J. Mater. Sci. Mater. Med.* **2007**, *18*, 1399–1405. [CrossRef]

56. D'Alessandro, D.; Perale, G.; Milazzo, M.; Moscato, S.; Stefanini, C.; Pertici, G.; Danti, S. Bovine bone matrix/poly(L-lactic-co-ε-caprolactone)/gelatin hybrid scaffold (SmartBone®) for maxillary sinus augmentation: A histologic study on bone regeneration. *Int. J. Pharm.* **2017**, *523*, 534–544. [CrossRef] [PubMed]